Nonlinear Froude-Krylov force modelling for two heaving wave energy point absorbers

Markel Peñalba Retes*, Alexis Mérigaud*, Jean-Christophe Gilloteaux[†] and John V. Ringwood*

*Center for Ocean Energy Research
Maynooth University, Co.Kildare, Ireland
mpenalba@eeng.nuim.ie
amerigaud@eeng.nuim.ie
john.ringwood@eeng.nuim.ie
[†]Ecole Centrale de Nantes, LHEEA Lab. (ECN/CNRS), Nantes, France
jean-christophe.gilloteaux@ec-nantes.fr

Abstract—**Most mathematical models used to assess the motions of wave-energy converters are linear, which may lead to significant errors as these devices can have a strongly-nonlinear behaviour. This paper investigates the effects of nonlinearities in the computation of Froude-Krylov forces, which play a major role in the dynamics of the motion of heaving energy point-absorbers, with a focus on the influence of the device's geometry. Results show that Froude-Krylov forces nonlinearities could be negligible when the device is uncontrolled. In contrast, they become significant when control is applied to maximise motions, especially for a device whose immersed cross-sectional area varies over time: in such a case latching control parameters based on a linear model can prove to be inefficient. Furthermore, although the latching control can be adapted to the nonlinear behaviour of the device by tuning parameters accordingly, the amount of power production assessed through the linear models does not seem to be achievable.**

Index Terms—**Wave energy, boundary element method, excitation force, Froude-Krylov force, nonlinear modelling**

I. INTRODUCTION

Mathematical models for wave energy devices are essential for power production assessment, for the simulation of device motion (including for control system assessment), or for the design of model-based control. They typically follow Cummins equation [1], using hydrodynamic parameters, identified in most of cases, by using boundary element methods (BEM). Most of these models are linear, which is attractive due to their low computational requirements. However, assumptions under which they are valid are restrictive, in particular the assumption of small motion.

In fact, the aim of wave energy converters (WEC) is to exaggerate the motion of the device to maximise the power production. Despite the objective to harvest energy, power absorption is not always possible, and other goals can be more important in specific situations, such as the safety of the device in extreme conditions. During survival mode, nonlinearities are high and important, but the machine may need to protect itself from the rough sea conditions and abandon power production.

However, it is also possible to meet situations where nonlinear effects are significant *within* the power production mode, as illustrated in Figure 1. This kind of situation is of particular interest for the present study, where the focus is on the impact of nonlinearities on the models developed for power production assessment and control design.
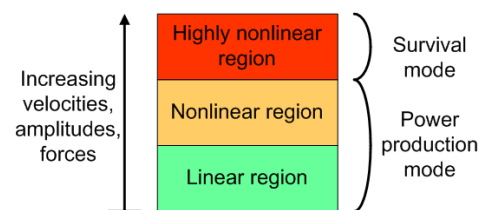
Fig. 1. Different operating regions for wave energy devices

Significant differences can be observed when comparing linear models to experimental tests [2] or nonlinear models [3]. As a consequence, linear models may need to be improved by adding appropriate nonlinear effects in order to have the fullest and most precise information possible about the system.

Well known and confirmed codes such as WAMIT [4], Aquaplus [5] or NEMOH [6], are based on boundary element methods and solve radiation and diffraction problems in the frequency domain, based on linear methods. However, nonlinear analysis requires time-domain simulations. As a consequence, frequency-domain results need to be adapted to be analysed in the time-domain, for example by using the Ogilvie's formula [7], or by performing simulations in the time-domain directly. The latter is used within the scope of this paper.

Different models have already been presented in the literature, where nonlinear effects have been added to the linear model, either using extended BEMs [3], [8], or by adding nonlinear forces to Cummin's equation [2], [9].

Froude-Krylov (FK) forces of heaving point-absorbers are the main component of the hydrodynamic force [3]. Therefore, in this paper, instantaneous static and dynamic Froude-Krylov forces are computed by using an extended BEM. Hence, integration of the hydrostatic force and incident wave dynamic pressure is performed over the exact instantaneous wetted surface. In order to further study the influence of the nonlinear FK forces, with regard to the geometry of the device, two different bodies are analysed: a sphere and a cylinder, both

with a single degree of freedom (heave). These geometries are chosen to offer one with a uniform cross-sectional area (CSA) and one with a non-uniform CSA. This choice will allow the investigation of the effect of variations in instantaneous wetted surface. For these two devices, the influence of nonlinear effects on the adequate setting of the control strategy and on power production is studied as well, in the specific and simple case of latching control.

II. THEORETICAL BACKGROUND OF BEMS

Two three-dimensional bodies are considered as floating wave energy converters, whose gravity centre at the hydrostatic equilibrium position is taken as origin point of the inertial reference frame. We assume the fluid to be inviscid and the incident flow to be irrotational and incompressible. That way, Newton's law can be used to specify the governing equation as follows:

$$m\ddot{\vec{x}} = \vec{F}_g - \iint_S P\vec{n}dS + \vec{F}_{PTO} \qquad (1)$$

where m is the mass of the body, x is the position of the body relating to its hydrostatic equilibrium position, F_g is the gravity force acting on the body, S the wetted surface, P the pressure acting on this surface, $\vec{n}$ the vector normal to the surface element and F_{PTO} the power take-off force, which will be modelled as a linear damper.

Potential theory is generally used in different BEM methods, where the potential flow of the wave describes the velocity field as the gradient of the velocity potential. This total flow can be divided into three different potentials: undisturbed incident flow (Φ_I), diffracted flow (Φ_D) and radiated flow (Φ_R). The sum of these three potentials makes up the total potential of the wave (Φ_{tot}).

$$\Phi_{tot} = \Phi_I + \Phi_D + \Phi_R \qquad (2)$$

The pressure P acting on the body can be obtained from the derivation of this total potential of the incident flow by using Bernoulli's equation:

$$P = -\rho gz - \rho\frac{\partial\Phi_{tot}}{\partial t} - \rho\frac{|\nabla\Phi_{tot}|^2}{2} \qquad (3)$$

where z is the position of the wetted surface and $-\rho gz$ the hydrostatic pressure acting on it.

A. Forces acting on the body

In the same way as the total potential is divided into three potentials in Eq. (2), the action of the pressure of each component of the potential can be identified and Eq. (3) can be written as follows:

$$P = -\rho gz - \rho\frac{\partial\Phi_I}{\partial t} - \rho\frac{|\nabla\Phi_I|^2}{2}$$
$$- \rho\frac{\partial\Phi_D}{\partial t} - \rho\frac{|\nabla\Phi_D|^2}{2}$$
$$- \rho\frac{\partial\Phi_R}{\partial t} - \rho\frac{|\nabla\Phi_R|^2}{2}$$
$$- \rho\nabla\Phi_I\nabla\Phi_R - \rho\nabla\Phi_I\nabla\Phi_D - \rho\nabla\Phi_D\nabla\Phi_R \quad (4)$$

where:

- $P_{st} = -\rho gz$ is the hydrostatic pressure as mentioned before, well known as Archimedes force. It forms the static Froude-Krylov force together with the gravity force (F_g):

$$\vec{F}_{FK_{st}} = \vec{F}_g - \iint_S P_{static}\vec{n}dS \qquad (5)$$

- $P_{dyn} = -\rho\frac{\partial\Phi_I}{\partial t} - \rho\frac{|\nabla\Phi_I|^2}{2}$ is the dynamic pressure, which generates the dynamic FK force:

$$\vec{F}_{FK_{dyn}} = -\iint_S P_{dyn}\vec{n}dS \qquad (6)$$

- $P_D = -\rho\frac{\partial\Phi_D}{\partial t} - \rho\frac{|\nabla\Phi_D|^2}{2}$ is the pressure related to the diffraction potential and generates the diffraction force:

$$\vec{F}_D = -\iint_S P_D\vec{n}dS \qquad (7)$$

- $P_R = -\rho\frac{\partial\Phi_R}{\partial t} - \rho\frac{|\nabla\Phi_R|^2}{2}$ is the pressure related to the radiation potential and generates the radiation force:

$$\vec{F}_R = -\iint_S P_R\vec{n}dS \qquad (8)$$

- $\rho\nabla\Phi_I\nabla\Phi_R$, $\rho\nabla\Phi_I\nabla\Phi_D$ and $\rho\nabla\Phi_D\nabla\Phi_R$ are second order diffraction-radiation terms.

As only Froude-Krylov forces are considered nonlinear in our model, quadratic terms in radiation and diffraction potentials and second-order terms are neglected. These terms are neglected in the same way by any other linear model.

Each of these individual forces contributes to the motion of the bodies and is shown in Eq. (9), which is the developed form of equation Eq. (1):

$$m\ddot{\vec{x}} = \vec{F}_{FK_{st}} + \vec{F}_{FK_{dyn}} + \vec{F}_D + \vec{F}_R + \vec{F}_{PTO} \qquad (9)$$

III. MODELLING METHODS

Two different models, based on BEM, are compared in this paper. The first one is the fully linear model while the second one is a weakly-nonlinear model that considers nonlinear Froude-Krylov forces.

A. Linear modelling

The linear method assumes that the amplitude and the steepness of the waves are small. Under this assumption, the fluid potential theory can be linearised and therefore, all the quantities of the simulation can be expressed over the mean wetted surface of the body. In addition, radiation and excitation forces are calculated by using the convolution integral of the corresponding impulse-response function and the velocity of the body (for radiation) or the free-surface elevation and (for the excitation term). Nevertheless, this time-domain approach has the same limitations as the frequency-domain simulation and so might be unable to accurately reproduce the motion of the body.

Under the linear approach, Eq. (9) is written as,

$$m\ddot{\vec{x}} = -K_H \vec{x} - \int_{-\infty}^{\infty} K_{Ex}(t-\tau)\eta(\tau)d\tau$$
$$- \mu_\infty \ddot{\vec{x}} - \int_{-\infty}^{\infty} K_R(t-\tau)\dot{\vec{x}}(\tau)d\tau - C_{PTO}\dot{\vec{x}} \quad (10)$$

where:

The static Froude-Krylov force is considered to act like a mass-spring system, where K_H is the hydrostatic stiffness matrix. This system represents the Archimedes force pushing up when the body is pushed down into the water and the gravity force pushing down when the body moves in the positive vertical sense.

The excitation force is formed by the dynamic Froude-Krylov force and the diffraction force and uses the convolution product between the excitation impulse-response matrix (K_{Ex}) and the free-surface elevation (η).

The radiation force is expressed by using the added mass term (μ_∞) and a convolution between the radiation impulse-response matrix (K_R) and the velocity of the body, according to the classical Cummins decomposition [1].

Power take-off force is modelled as a linear damper using a fixed damping coefficient (C_{PTO}).

Time-domain hydrodynamical coefficients and impulse-response functions (K_H, K_{Ex} and K_R) are directly given by ACHIL3D [10] calculations.

However, this linear approach neglects significant nonlinearities such as the second order terms of the Eq. (4), nonlinearities of the incident waves, or geometric nonlinearities generated by pressure forces acting over a varying wetted surface. The method presented in Section III-B is designed to deal with variations in wetted surface.

B. Nonlinear Froude-Krylov forces

In order to improve the accuracy of the linear model, another degree of complexity can be introduced to extend the linear approach. Instead of using the mean wetted surface, the undisturbed incident wave pressure as well as the hydrostatic force can be integrated over the *instantaneous* wetted surface. It implies that the wetted surface will change over time and so will need to be re-defined at each time-step, which has been applied in few models showing very promising results [2], [3], [11]. Calculating instantaneous wetted surface requires an additional computational effort, especially since it implies the use of a very fine mesh that takes into account only those cells of the mesh below the instantaneous free surface [2] or an automatic remeshing routine [3], [11] as applied in this paper's framework.

Eq. (10) can be written as

$$m\ddot{\vec{x}} = \vec{F}_g - \iint\limits_{S(t)} (P_{st} + P_{dyn})\vec{n}dS - \int_{-\infty}^{\infty} K_D(t-\tau)\eta d\tau$$
$$- \mu_\infty \ddot{\vec{x}} - \int_{-\infty}^{\infty} K_R(t-\tau)\dot{\vec{x}}(\tau)d\tau - C_{PTO}\dot{\vec{x}} \quad (11)$$

where:

The Froude-Krylov forces are integrated over the instantaneous wetted surface. In our case, an automatic remeshing routine, explained in detail in [8], is used to compute the exact instantaneous wetted surface. This routine first involves the computation of the intersection between the body and the free surface, then the selection of the immersed or partially immersed panels and, finally, the remeshing of those panels that are partially immersed.

The diffraction force is expressed by the convolution product between the diffraction impulse-response matrix (K_D) and the free-surface elevation (η). In this case the diffraction force remains linear as in the linear approach, but it is analysed independently. K_D is also computed by ACHIL3D code.

The radiation force is computed as in the linear approach.

The power take-off force remains the same as in the linear approach.

IV. CASE STUDY

The main objective of this paper is to assess the relevance of modelling nonlinear Froude-Krylov forces with regards to the geometry of a device. Therefore, two shapes are studied: a sphere and a cylinder. Sphere has a varying CSA, which is likely to increase the effects of geometric nonlinearities, while cylinder has a constant CSA, which could make the linear model a better approximation than it is for the sphere case, at least when the motion amplitude of the cylinder does not exceed its length.

Only heave motion is considered for both devices, in order to simplify the analysis, assuming, in both cases, that the bodies are tethered to the seabed with power take-off (PTO) systems based on a linear damper. Figure 2 shows the configuration of the two cases.

This section explains how the dimensions of these two devices are set, presents the range of sea states in which their dynamic behaviour is simulated, and describes the power take-off and control strategies that are used.
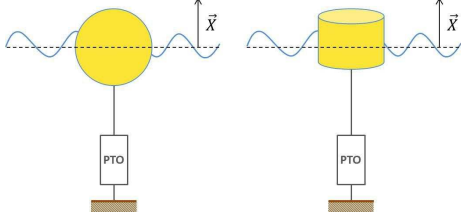
Fig. 2. Sketch view of the two configurations: sphere and cylinder.

A. Body geometries

As a previous study utilised a sphere [3] and results showed the significance of the nonlinear Froude-Krylov forces, a sphere is retained. However, the dimensions are different in this case, to be as close as possible to realistic device parameters.

The dimensions of the cylinder are defined so as to present as much comparability as possible with the sphere. First of all, the two devices are chosen to have a density of $500kg/m^3$, so that the positions of their gravity centres at hydrostatic equilibrium are the same and aligned with the free surface at rest, and so that the asymmetries of their vertical motions are limited. Furthermore, the condition that the two devices should have a similar natural frequency is chosen as a comparability criterion. In addition, it can be useful to keep similar geometric dimensions like radius, draft or volume displacement, in order to obtain forces of similar magnitude acting on the two bodies. All these choices are designed to make the results easier to compare.

Requirements to make the bodies comparable lead to the choice of a 5-m diameter sphere (inspired by real-life wave energy devices such as the WAVESTAR device [12]) with a density of $500kg/m^3$, as mentioned above. In order to find dimensions for the cylinder that meet the chosen comparability criteria, basic algebraic calculations are used, based on the typical equations for the natural frequency (ω_0) shown in Eq. (12) for the sphere and in Eq. (13) for the cylinder:

$$\omega_0 = \sqrt{\frac{\rho g \pi R_s^2}{\rho \frac{4}{3} \pi R_s^3 (1+\varepsilon)}} = \sqrt{\frac{3g}{4R_s(1+0.5)}} \quad (12)$$

$$\omega_0 = \sqrt{\frac{\rho g \pi R_c^2}{\pi \rho R_c^2 2H_c + \frac{4}{3}\rho R_c^3}} = \sqrt{\frac{\pi g}{\pi H c + \frac{4}{3}Rc}} \quad (13)$$

For a sphere of radius R_s, the added mass is calculated by using an approximation, where $\varepsilon = 0.5$ [13]. For a cylinder of radius R_c and draft H_c, the added mass is calculated by using the well-known analytical formula $A_\infty = \frac{4}{3}\rho R_c^3$ [14].

Hence, for a sphere having a natural period of 3.17s, according to Eq. (12), suitable geometric characteristics for the cylinder can be found using the formula in Eq. (13)

so as to obtain the same natural period. This results in a rather flat cylinder with the same radius as the sphere and a similar displacement. Table I summarizes all the geometric characteristics of the two bodies.

TABLE I
GEOMETRICAL CHARACTERISTICS OF THE BODIES

	Sphere	Cylinder
Geometry		
Radius (m)	2.5	2.5
Draft (m)	-	1.45
Displacement (m^3)	32.72	28.47
Natural period (s)	3.17	3.17
Optimal PTO damping (B_{PTO})	25000	26000

Once the geometric features of the devices are set, ACHIL3D simulations are run in order to obtain the hydrodynamic parameters needed in the two time-domain hydrodynamic modelling methods.

B. Sea-states

The response amplitude operator (RAO) of a given wave energy converter allows for a representation of its behaviour under the whole range of wave periods. Knowledge of the RAO is of high importance with regard to the power output and motions that can be expected, both in usual operating conditions and in extreme sea states. Yet, taking nonlinearities into account in the modelling of the WECs motions could generate significant changes in its expected response.

That is why the RAOs are plotted for the two devices using both hydrodynamic models described in Section III, serving as a relevant point of comparison.

To achieve this, simulations must be run for many different monochromatic wave periods. The studied devices are assumed to operate under deep water conditions, which is consistent with their dimensions and with the wave characteristics used in the simulations. Under deep water assumption, the wave length (λ) and period (T) are related as follows:

$$\lambda = \frac{g}{2\pi}T^2 \quad (14)$$

Hence, the choice of a wave period determines the wavelength. In order to study the responses of the device for different wave periods and compare them easily, the same wave steepness is kept for all the simulations. As a consequence, for each wave period T_W the wave height H is set so that the steepness $\frac{H}{\lambda}$ remains constant.

As our primary goal is to study the effects of nonlinear *device modelling* only, and not those of nonlinear wave modelling, regular, linear waves based on Airy's theory are used. This is a good approximation for relatively small and flat waves. The wave steepness $\frac{H}{\lambda}$ is set to 0.018, based on a wave of 1m height and 6s period (λ is then $56.25m$). These parameters could correspond to realistic typical wave

conditions and describe normal operating conditions for our WECs.

Table II shows the range of wave periods and their corresponding wave heights and wavelengths in function of the selected steepness value.

TABLE II
ANALYSED SEA-STATES FOR THE 0.018 STEEPNESS

Wave periods [s]	3	4	5	6	7	8	10
Wave height [m]	0.25	0.44	0.69	1	1.36	1.78	2.78
Wavelength [m]	14	25	39	56	77	100	156

C. Power absorption and control

The main objective of a WEC is harvesting power from the waves. The absorption rate depends on the velocity of the device, among others aspects such as PTO system, mooring lines or the geometry of the device. In order to assure amplified motions even when the wave frequency is far from the natural frequency of the device, the velocity of the device can be regulated by using control strategies, adapting the device to the incident wave. This adaptation can considerably increase the power capture, improving it by a factor 2 in irregular waves and 4 in regular waves [15] using latching control. This latter control strategy is chosen for this work, due to its simplicity and efficiency [16].

1) Latching control strategy: Latching control consists of locking the motion of the device when its velocity goes to zero, and keeping it latched until the wave force reaches the most advantageous phase, when the device will be unlatched. The motion of the device is then a succession of ramps separated by periods of rest, as illustrated in Figure 3.
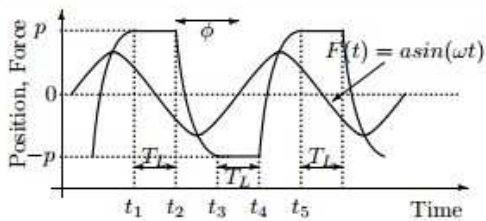

Fig. 3. Latching calculations, [16]

The control variable is the duration of the latching period (T_L), calculated using the natural period of the device (T_{ω_0}) and the period of the incident wave (T_W) as follows:

$$T_L = \frac{t_5 - t_1}{2} - (t_5 - t_4) = \frac{T_W}{2} - \frac{T_{\omega_0}}{2} \quad (15)$$

If the natural period of the device is known, and regular, monochromatic waves are used, this optimal latching time is easy to compute and remains constant over time. An initial latching control strategy (hereafter referred to as fixed-time latching strategy) can then be defined based on linear theory: (T_L) is kept constant and is defined as in the equation above.

This fixed-time control strategy is designed to give very good results in the scope of linear theory, where the natural period of the device is indeed very well-defined, since it only depends on the hydrostatic stiffness, mass and added mass of the device, as described in Section IV-A. But it may not be the best strategy with the weakly-nonlinear model since, in this case, the device does not have a clearly-defined hydrostatic stiffness, especially when the immersed CSA of the device is not constant. This will be confirmed by the results presented in Section V.

A second latching control strategy (hereafter referred to as adaptive latching strategy) is then defined, in which a basic algorithm, presented in Figure 4, allows for adaptive changes in the latching period in order to obtain the greatest possible motion amplitude in the incident monochromatic wave train, regardless of the hydrodynamic model that is used.

The adaptive algorithm consists of modifying the latching period step-by-step in a direction that increases the motion amplitude. Between two consecutive modifications, the algorithm waits for the motion to reach a steady state in order to get a reliable evaluation of the new motion amplitude obtained. Dealing with monochromatic waves, the criterion used to determine if this steady state is reached is to check whether the motion period is close enough to the wave period. The algorithm then alternates modifications of the latching period and stabilisation phases.

In Figure 4, T_m is the period of the device's motion, measured as twice the time elapsed between two consecutive latching events, l is the threshold which determines whether the motion has reached the steady state situation, A^* is the memorised motion amplitude obtained with the previous latching time, and d is the increment to the latching time.

Unlike the constant latching time used in the strategy based on the linear model, this adaptive algorithm enables the device's motion to reach a pattern which is well-synchronised with the excitation force, even when using the weakly-nonlinear hydrodynamic model, thus ensuring that motion amplitude and power production are the best that can be obtained by using latching in monochromatic waves. Notice that when applied to the linear hydrodynamic modelling case, the algorithm converges to the initial latching control strategy.

2) Power Take-Off: For reasons of simplicity and generalisation capability, in this paper the PTO system is modelled as a linear damper, as illustrated in Figure 2. The optimal value for the PTO damping coefficient of each device is calibrated using linear simulations. When using latching, this optimal PTO value shows very little sensitivity to the incoming wave period. That's why a single PTO damping value is defined for each device, which allows for a good power capture in all the studied sea states, while facilitating efficient comparisons. Values for (B_{PTO}) are presented in Table I.

V. RESULTS

Results are obtained by using a program written in Fortran that performs the time-domain simulation of the device's motion (using 4th-order Runge-Kutta integration) and has the
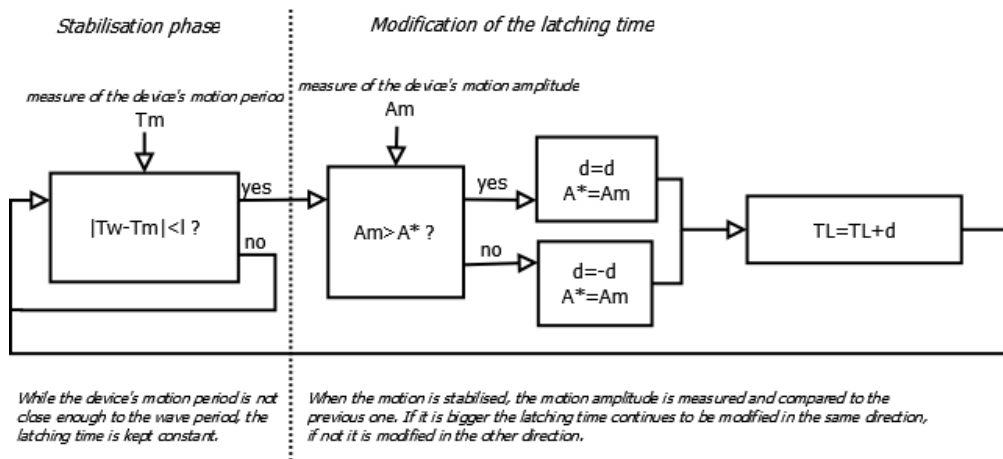
Fig. 4. Diagram of the algorithm for the new latching strategy created to apply with nonlinear FK forces

ability to compute nonlinear Froude-Krylov forces such as described in Section III-B. Initially, the ACHIL3D software is used to generate the hydrodynamic coefficients which will be used for each geometry in all the simulations.

The only nonlinear effects analysed are Froude-Krylov forces, as [3] identifies them to be mainly responsible for the nonlinear behaviour of point absorbers. The rest of the forces (radiation, diffraction, incident wave, ...) are modelled using linear models.

Various simulations are run to compare linear and nonlinear models for the two devices described in Section IV-A: a very simple free-decay case is briefly studied, where only the static part of the FK forces is active, in order to validate this paper's basic hypothesis about the impact of the device's geometry. Simulations are then performed over a range of linear monochromatic waves such as described in Section IV-B, first in the case where the device goes uncontrolled, then using the two different latching control strategies described in Section IV-C. It is then ensured that nonlinear behaviours are represented under a wide range of conditions.

A. Free-decay

For the free-decay simulation, the initial position of the body is set where the devices are immersed below their equilibrium position, so that their motion is then a damped oscillation around their equilibrium position.

One can very quickly notice, in Figure 5, how the nonlinear curve stays exactly on top of the linear curve for the cylinder, while there is a visible difference in the case of the sphere.

Differences observed between linear and weakly-nonlinear models in the case of the sphere are due to the computation of the instantaneous wetted surface in the nonlinear simulation, which, in this case, leads to a non-constant immersed CSA, resulting in lower amplitudes and slower dynamics. In contrast, the immersed CSA remains constant for the cylinder; as a consequence, the hydrostatic stiffness coefficient used in the linear method to model static FK forces is a good approximation, and that is why both simulations give identical results.
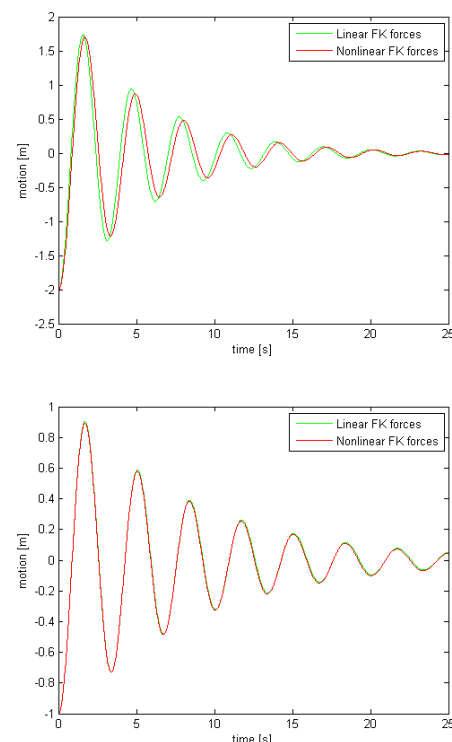

Fig. 5. Free-decay simulations for sphere (on top) and cylinder (below)

The free-decay test highlights the geometrical nonlinearities of the sphere in comparison with the cylinder and suggests that the influence of the nonlinear FK forces can be more significant in the case of the sphere.

B. Uncontrolled motions in regular waves

Although the free-decay test already highlighted the nonlinear behaviour of the sphere it is, of course, more interesting to analyse the responses of the devices in various incident wave trains. As mentioned in Section IV-B, only linear, regular

waves are used, as the main objective is to focus on the FK force nonlinearities.
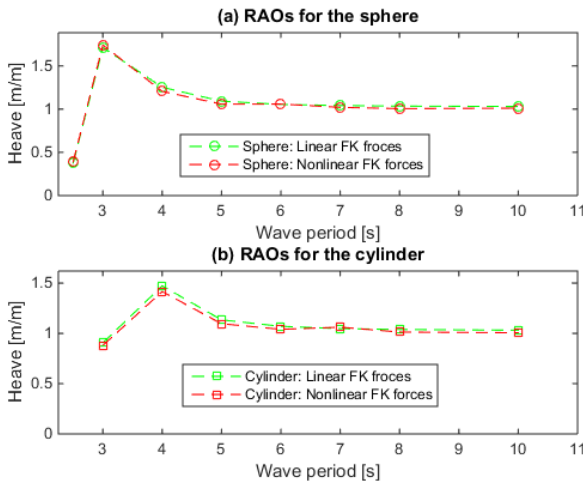

Fig. 6. RAOs of linear and nonlinear uncontrolled simulations for the sphere on top and the cylinder below for different incident wave trains

The responses of the devices are first analysed by plotting RAOs for the case where they move freely, without any control or PTO system damping. Figure 6(a) and 6(b) show the results for the sphere and the cylinder respectively, for different wave periods and amplitudes. There is very little difference between the linear and nonlinear computation of FK forces, the nonlinear case showing a barely lower RAO than the linear one, even for big waves.

This result is explained as follows: the natural frequency of the device is between 3 and 4 s in both cases. But waves whose periods are close to these values, have small heights (as shown in Table II) compared to the dimensions of the devices. Therefore, for wave periods close to their natural resonant frequency, the devices do resonate and have greater motions than the incident waves; however, the motion amplitude in relation to the water surface is too small compared to the device's dimensions to see any significant geometric nonlinear effects (about 0.2 m of amplitude while the drafts of the devices are 2.5 and 1.45m respectively). In contrast, bigger waves are those whose periods are well above the natural period of the devices. Thus, the WECs do not resonate, and behave as wave-followers: as a consequence the motions, in relation to the water surface, are again very small compared to the device's dimensions.

C. Controlled motions in regular waves

The results of the control- and PTO-free case for these specific devices do not especially highlight the interest of modelling nonlinear features of the FK forces. However, a realistic wave-energy device would be likely to be equipped with a control system, enabling it to exaggerate its motions not only in small waves, but also in bigger ones that are away from its natural period. As a consequence, the latching

control strategies defined in Section IV-C1 are applied to the two devices.

1) Fixed-time latching strategy: The fixed-time latching strategy is suitable when the immersed CSA and the wetted surface can be assumed to be constant. However, as soon as CSA and wetted surface start to vary significantly over time, as made possible by the weakly-nonlinear model, this latching strategy loses efficacy.
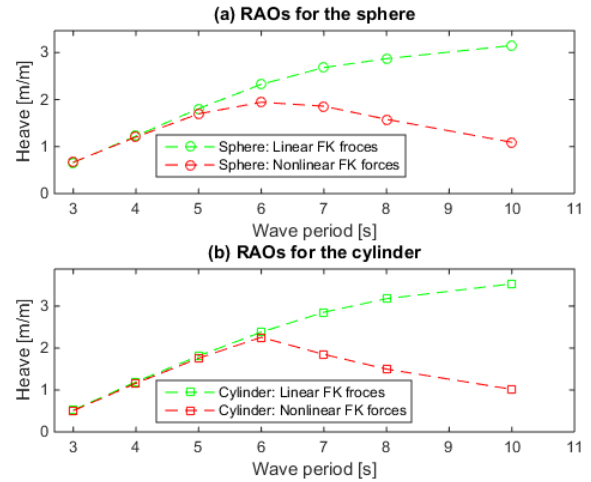

Fig. 7. RAOs of linear and nonlinear computations for the sphere on top and the cylinder below for different incident wave trains in controlled simulations using the fixed-time latching strategy

Figure 7 demonstrates the loss of effectiveness of the fixed-time latching strategy for the two devices. While the control seems to work efficiently in small waves (up to about 6s wave periods, i.e. 1-m wave height), its performance drops dramatically in bigger waves, when nonlinearities become significant.

The loss of efficacy of the fixed-time latching strategy when using the weakly-nonlinear model can be more precisely understood by analysing the motion of the device in a given wave, as shown in Figures 9(a) and 9(b), which illustrate how this control strategy works well using the linear model, but is totally inadequate when nonlinear FK forces become significant: the latching time is then poorly adapted to the slower nonlinear dynamics of the device. Thus, the fixed-time latching strategy is not able to place the velocity profile in phase with the excitation force profile. Figure 9 shows $20s$ of the steady state of a simulation with a wave period of $8s$.

As seen in Figure 7, the bigger the wave, the more inadequate the control strategy, since nonlinearities are more significant. Using an inadequate control strategy has an adverse effect on the motion of the device, and in consequence, on the power production.

In order to focus on the differences between the sphere and the cylinder, the relative difference of the motion RAOs between linear and weakly-nonlinear models is computed for the two geometries and shown in Figure 8.
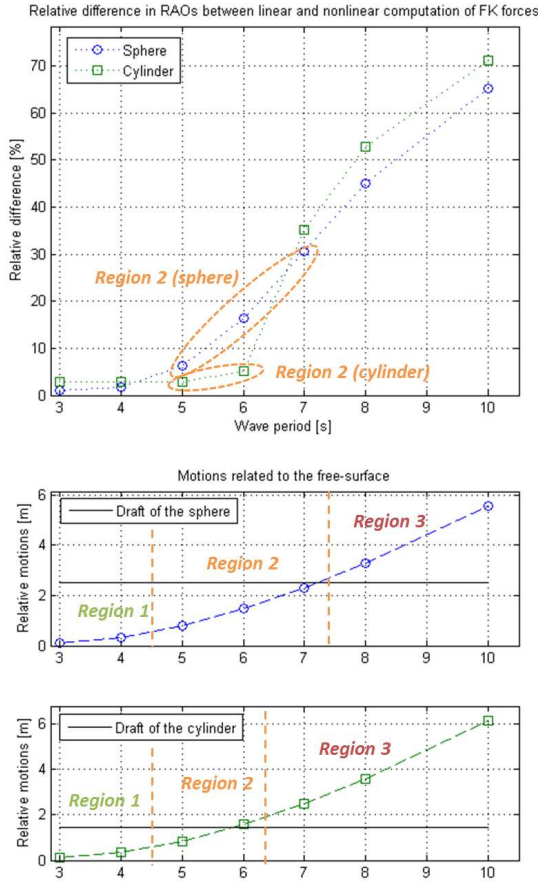
Fig. 8. On top, relative difference in RAOs between linear and nonlinear simulations. Below, amplitude of the relative motion between the device and the free-surface, compared to the drafts of the devices, for the sphere and the cylinder. The three regions are shown in all of them

Denoting the amplitude of the motion in relation to the free surface as A_W and the draft of the device as D, based on Figure 8, three important types of situations can be depicted, in which the differences between linear and nonlinear simulations are significant or not, for each device:

- *Region 1*, $A_W << D$ (wave periods below 5s for both devices): For the sphere and for the cylinder, the nonlinearities in the computation of FK forces, especially geometric nonlinearities, are insignificant and thus have very little impact on the dynamics of the device. The linear model is then a good approximation, and the fixed-time latching strategy, which is based on the linear model, works well even in the simulations using the weakly-nonlinear hydrodynamic model.
- *Region 2*, $A_W < D$ (wave periods of 5 to 6s for the cylinder, 5 to 7s for the sphere): The linear model fails to accurately describe the motion of the sphere, but remains accurate for the cylinder, whose immersed CSA is constant. Thus, the fixed-time latching strategy applied to the weakly-nonlinear model looses efficiency for the sphere but keeps good performance for the cylinder.

- *Region 3*, $A_W > D$ (wave periods above 7s for the cylinder, above 8s for the sphere): Because of bigger wave heights, combined with the motion being magnified by the latching, the devices spend a significant amount of time either fully submersed, or totally out of the water. As a consequence, the immersed CSA cannot be assumed to be constant any more, either for the sphere or for the cylinder, and the linear model becomes a poor approximation for both shapes. The performance of the fixed-time latching strategy drops accordingly when applied to the nonlinear model.

While the realism of the situations described in *Region 3* could be rightfully questioned, *Region 2* is of particular interest, since it corresponds to typical wave conditions such as those described in Figure 8, and results in motions of very significant amplitude. These significant motions demonstrate the existence of realistic operational conditions in which nonlinear effects cannot be neglected, especially when dealing with a device whose immersed CSA is not constant. Nonlinear effects have, in addition, a significant impact on the efficiency of the control strategy. A control strategy based on the linear model can prove to be inefficient when applied to a device whose behaviour is nonlinear.

Note that *Region 2* in Figure 8 is smaller for the cylinder than it is for the sphere; this is because of its relatively small draft due to the conditions chosen to enhance comparability between the two devices. Using a taller device, the range within which the linear model accurately represents the cylinder's dynamics may be increased.

2) Adaptive latching strategy: The importance of nonlinearities in the setting of the control strategy is now demonstrated. However, another question arises: if one succeeds in consequently adapting the control strategy to the nonlinear characteristics of the motion, can one expect to harvest as much power as promised by the linear model? This subsection attempts to give a part of the answer to this question.

The control strategy needs to be improved in order to maximize power production in all waves, including when using the model with nonlinear Froude-Krylov forces. This is why the adaptive latching control strategy, presented in Section IV-C and based on an algorithm to find the optimal latching time, is implemented. Due to its very simple features, the algorithm of the adaptive latching strategy is not designed to represent a real-time controller. What matters is the ability of the adaptive latching strategy to place the device's velocity pattern well in phase with the excitation force - just as the first latching strategy does in the linear case. One can then reasonably compare the power outputs that are to be expected when using the linear and weakly-nonlinear models.

Figures 9(b) and 9(d) clearly illustrate the improvement brought to the control strategy by the adaptive algorithm, the velocity of the device now being in phase with the excitation force. The adaptive latching strategy, in the case of nonlinear FK forces computation, results in an optimal latching time T_L' which is different from the fixed-time latching period T_L. When the adaptive strategy is applied in the linear simulations,
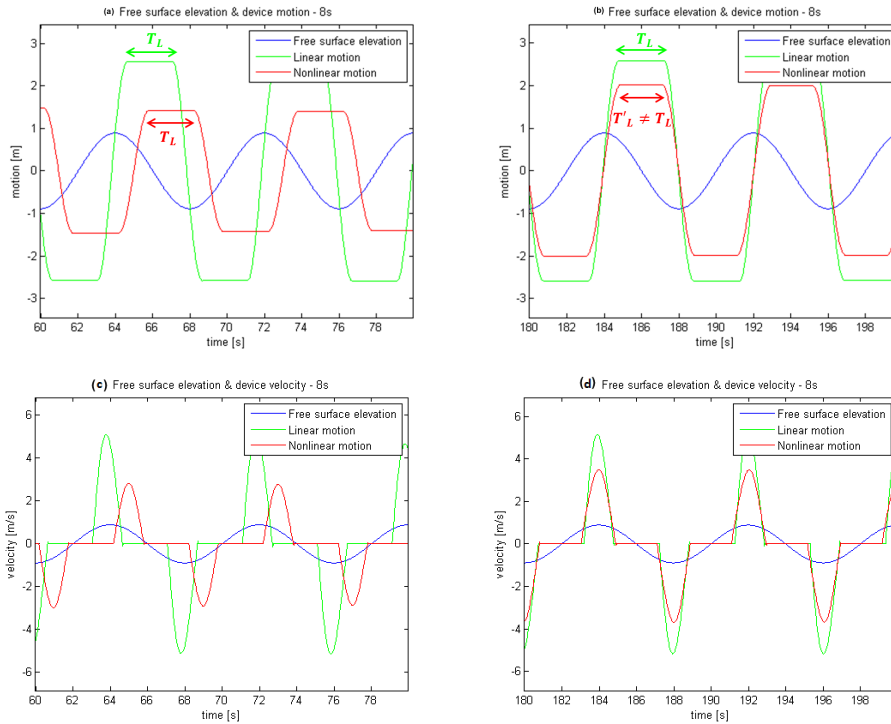
Fig. 9. Motion amplitude on top and velocity below of the sphere, for the controlled case using the fixed-time strategy on the left and the adaptive strategy on the right

the optimal latching period converges to T_L so that the motions end up being the same as with the fixed-time latching strategy, as green lines in Figure 7 and 10 illustrate.
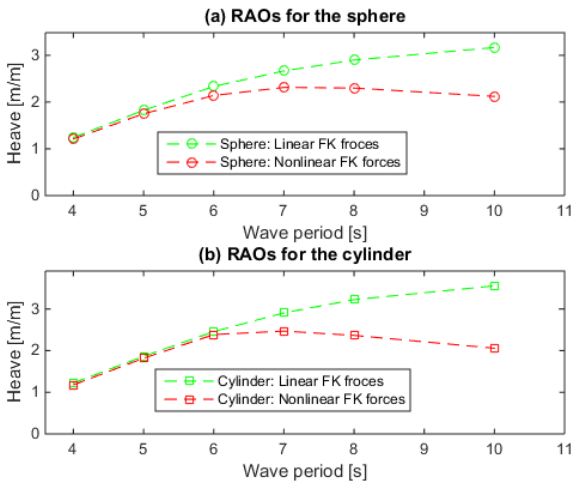

Fig. 10. RAOs of linear and nonlinear computations for the sphere on top and the cylinder below for different incident wave trains in controlled simulations using the adaptive latching strategy

As a result, the motion amplitude obtained with the weakly-nonlinear model is increased, now being closer to the one obtained with the linear model. However, there still remains a gap between the linear and weakly-nonlinear cases.

The new motion RAOs are plotted in Figure 10, which illustrates both the improvement brought by the adaptive control strategy in the case of the weakly-nonlinear model, as well as the significant remaining difference between the results obtained, depending on whether linear or nonlinear FK forces are computed.
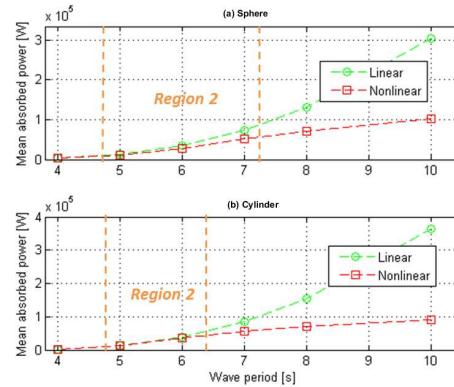

Fig. 11. Mean absorbed power by the sphere on top and the cylinder below

The consequences of FK force nonlinearities on power absorption are illustrated in Figures 11 and 12, which both show a lower efficiency in the nonlinear case. Using the adaptive latching strategy, Figure 11 represents the mean power ($P = \frac{1}{2} B_{PTO}|v|^2$) absorbed by both devices in the linear and weakly-nonlinear cases. Figure 12 represents an estimation of the power output (in $\%$), i.e. the mean absorbed
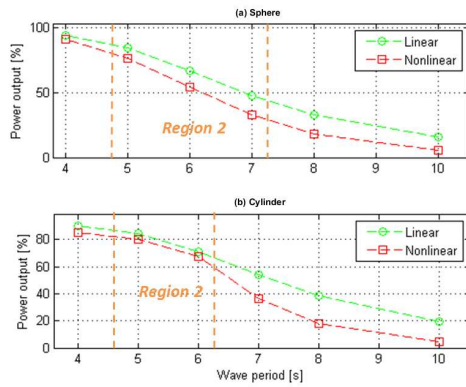
Fig. 12. Relative difference in mean absorbed power between linear and nonlinear computation of FK forces

power ($P = \frac{1}{2}B_{PTO}|v|^2$) divided by the theoretical maximum wave power that can be captured by a heaving axisymmetric point-absorber in deep waters $P_{Max} = \frac{1}{8}\rho g H^2 C_g \frac{1}{k}$ where C_g is the group velocity, $\frac{1}{8}\rho g H^2 C_g$ (in W/m) is the wave power per unit of wave crest and $\frac{1}{k} = \frac{\lambda}{2\pi}$ (in m) is the absorption width. It seems, from these results, that even when the latching time is tuned to the nonlinear behaviour of the device, the resulting power output is significantly lower than the one that can be assessed through linear simulations.

VI. CONCLUSION

It appears, from the results of this study, that nonlinearities of FK forces are not consistent in the forced, uncontrolled case. In addition, the results obtained for the cylinder tend to show that when the immersed CSA of the device is constant, linear models can remain accurate (as far as Froude-Krylov forces are concerned) provided that the amplitude of the motion in relation to the free-surface elevation does not exceed the dimensions of the body. However, the range of conditions under which linear models remain realistic should be further investigated by using a taller cylinder than the one modelled in this study.

In contrast to the uncontrolled case, nonlinear effects become significant when control is used, especially with a device whose immersed CSA presents noticeable variations over time. In such cases, nonlinear effects have important implications for the models that should be used in control design, as well as for power capture assessment. Firstly, a control system based on a linear model can prove to be inefficient when applied to a device whose motions show significant nonlinearities in normal operating conditions - such as the sea states examined in this paper. Secondly, power capture assessment using linear FK models can be unreasonably optimistic and give a misleading guide on the economic value of a device.

It has to be noted that the waves used in the simulations presented in this paper are linear and thus are relatively flat waves. Taking into account steeper, nonlinear waves, such as those which can be encountered in real sea conditions, would be likely to enhance the nonlinear effects described, along with

their impact on control design and power production assessment. Furthermore, only heave motions have been considered in the present work, while higher nonlinear effects could be expected by adding more degrees of freedom, due to their coupling.

Finally, the presented formulation of the nonlinear FK forces does not lend itself easily to model-based control design and further work is necessary to develop corresponding nonlinear control algorithms capable of real-time operation. However, control strategies based on latching can be tuned adaptively and do not depend on the hydrodynamic model adopted.

REFERENCES

[1] W. Cummins, "The impulse response function and ship motions," vol. 9 (Heft 47), pp. 101–109, June 1962.
[2] A. Babarit, P. Laporte-Weywada, H. Mouslim, and A. H. Clement, "On the numerical modelling of the nonlinear behaviour of a wave energy converter," in *Procedings of the ASME 28th Intl. Conf. on Ocean, Offshore and Artic Engineering, Honolulu, OMAE*, vol. 4, May-June 2009, pp. 1045–1053.
[3] A. Merigaud, J. Gilloteaux, and J. Ringwood, "A nonlinear extension for linear boundary element method in wave energy device modelling," in *In Proceedings of the 31st Intl. Conf. on Ocean, Offshore and Artic Engineering (OMAE), Rio de Janeiro*, 2012, pp. 615–621.
[4] M. WAMIT Inc., *WAMIT v7.0 manual*, 2013.
[5] G. Delhommeau, "Seakeeping codes aquadyn and aquaplus," in *In Proc. of the 19th WEGEMT School on Numerical Simulation of Hydrodynamics:Ships and Offshore Structures, Nantes*, 1993.
[6] *NEMOH software*. [Online]. Available: https://lheea.ec-nantes.fr/doku.php/emo/nemoh/start
[7] T. Ogilvie, "Recent progress toward the understanding and prediction of ship motions," in *Proc. of the 5th Symposium on Navan Hydrodynamics, Bergen, Norway*, ser. ONR, vol. ACR-112, 1964, pp. 3–79.
[8] J.-C. Gilloteaux, "Mouvements de grande amplitude d'un corps flottant en fluide parfait. application a la recuperation de l'energie des vagues," Ph.D. dissertation, Ecole Centrale de Nantes (ECN), 2007.
[9] A. Zurkinden, F. Ferri, S. Beatty, J. Kofoed, and M. Kramer, "Nonlinear numerical modelling and experimental testing of a point-absorber wave energy converter," *Ocean Engineering*, vol. 78, pp. 11–21, 2014.
[10] A. Babarit, *Achil3D v2.011 User Manual.*, Laboratoire de Mécanique des Fluides CNRS, Ecole Central de Nantes, 2010.
[11] J.-C. Gilloteaux, G. Bacelli, and J. Ringwood, "A nonlinear potential model to predict large-amplitude-motions: Application to a multy-body wave energy converter," in *In Proc. 10th World Renewable Energy Conference, Glasgow*, 2008.
[12] "Wavestar website," www.wavestarenergy.com. [Online]. Available: http://wavestarenergy.com/
[13] J. N. Newman, *Marine hydrodynamics*. MIT press, 1977.
[14] O. Faltinsen, *Sea Loads on Ships and Offshore Structures*, ser. Cambridge Ocean Technology Series. Cambridge University Press, 1993.
[15] A. Babarit and A. Clément, "Optimal latching control of a wave energy device in regular and irregular waves," *Applied Ocean Research*, vol. 28, no. 2, pp. 77–91, 2006.
[16] J. V. Ringwood and S. Butler, "Optimisation of a wave energy converter," in *Proc. IFAC Conf. on control application sin Marine Systems, Ancona, Italy*, 2004.